Supplementary Information

Mobile Health (mHealth) Viral Diagnostics Enabled with Adaptive Adversarial Learning

Ahmed Shokr,[‖,#] Luis G. C. Pacheco,[‖,‡,#] Prudhvi Thirumalaraju,[‖,#] Manoj Kumar Kanakasabapathy,[‖,#] Jahnavi Gandhi,[‖] Deeksha Kartik,[‖] Filipe S. R. Silva,[‖,‡] Eda Erdogmus,[‖] Hemanth Kandula,[‖] Shenglin Luo,[‖] Xu G. Yu,[£,¥,†] Raymond T. Chung,[§,†] Jonathan Z. Li,[¥,†] Daniel R. Kuritzkes,[¥,†] and Hadi Shafiee[‖,†,*]

[‖]Division of Engineering in Medicine, Department of Medicine, Brigham and Women's Hospital, Harvard Medical School, Boston, MA, 02139, USA.

[‡]Department of Biotechnology, Institute of Health Sciences, Federal University of Bahia, Salvador, BA, 40110-100, Brazil.

[£]The Ragon Institute of Massachusetts General Hospital, Massachusetts Institute of Technology and Harvard University, Boston, MA, 02129, USA.

[¥]Division of Infectious Diseases, Brigham and Women's Hospital, Harvard Medical School, Boston, MA, 02139, USA.

[§]Liver Center, Gastrointestinal Division, Massachusetts General Hospital, Harvard Medical School, Boston, MA, 02114, USA.

[†]Harvard Medical School, Boston, MA, 02115, USA.

* Corresponding author: Hadi Shafiee, E-mail: hshafiee@bwh.harvard.edu

[#] These authors contributed equally.

Table of Contents

Supplementary Figures

Supplementary Tables

Table S4. List of antibodies, oligonucleotides, and synthetic nucleic acids used in this study

Supplementary Videos

Supplementary Videos S1-S5. The degree of microchip images separability in a 3D space, visualized by t-distribution stochastic neighbor embedding (t-SNE)

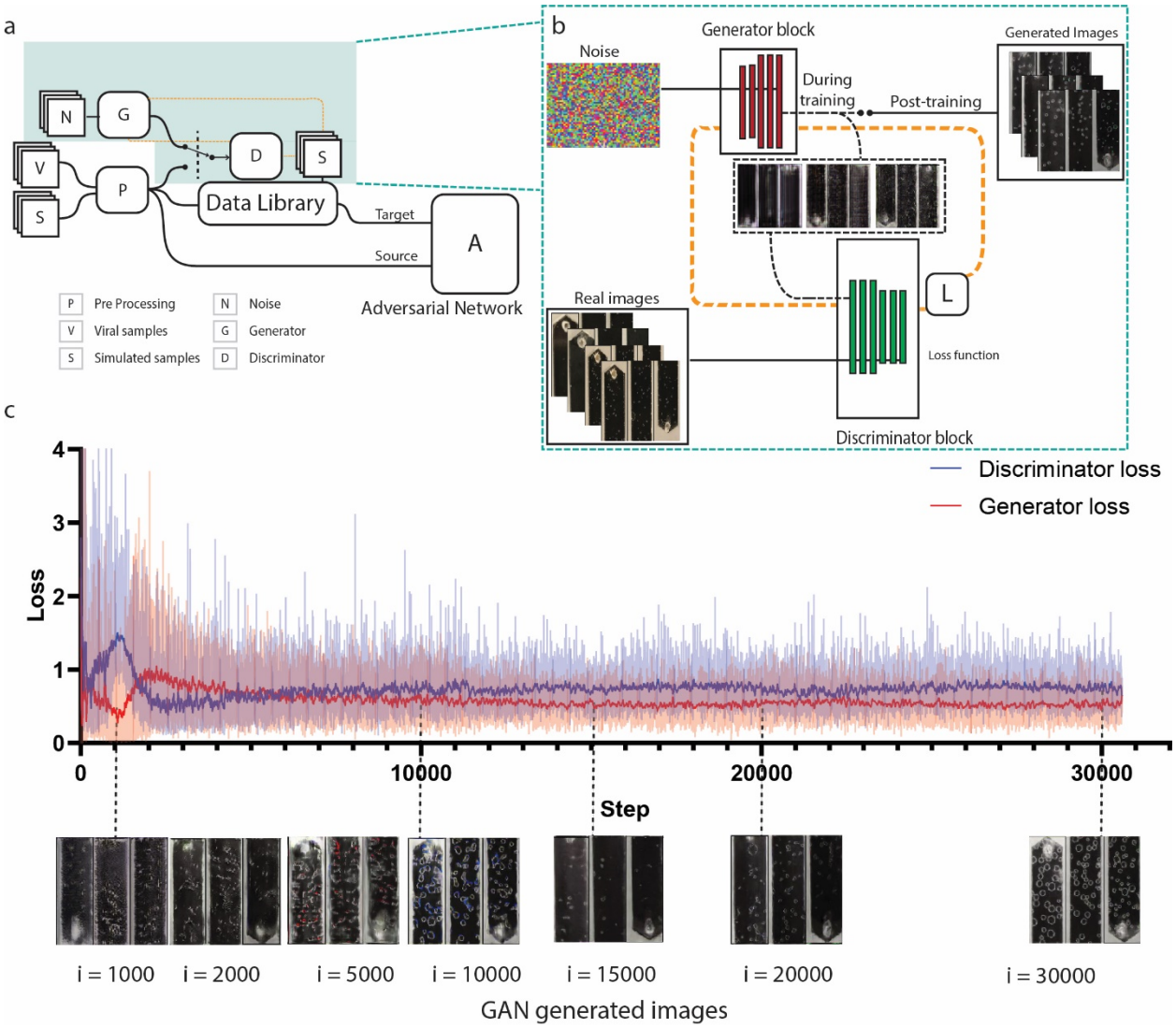

Figure S1. Construction of the microchip image database containing real microchip images and synthetic images generated using style generative adversarial networks (StyleGANs). a, The microchip image dataset is composed of 17,573 unique images, originated form real smartphone-taken microchip images from virus detection assays (n = 669) or simulated non-specific samples (n = 904), and synthetic images generated using StyleGANs (n= 16,000). **b**, Schematic of the adversarial learning architecture. The synthetic image dataset was generated using a styleGAN trained and developed using the real microchip images, both the ones originated from true virus detection assays and the simulated microchip images. **c**, Generator and discriminator loss over time.

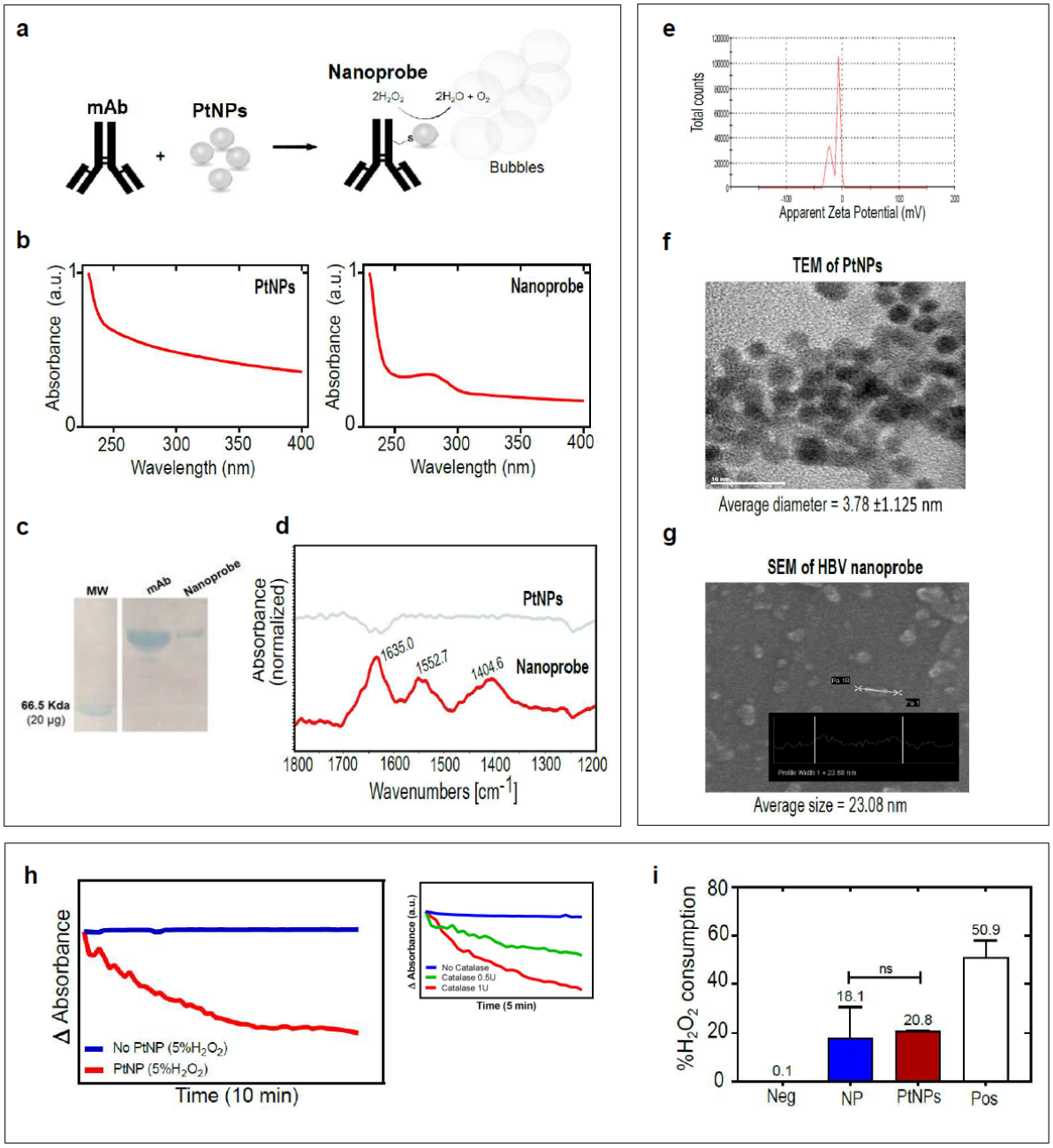

Figure S2. The basics of fabrication and functioning of the target-specific nanoprobes. a, Overview of the nanoprobe fabrication protocol. **b**, UV-Vis spectroscopy of platinum nanoparticles (PtNPs) (left panel) and an anti-HBV nanoprobe (right panel). There was a high optical absorption at lower wavelengths in both solutions, as expected for the presence of PtNPs (absorption peaks around 212 – 260 nm). A second distinctive peak around 280 nm was seen in the filtered nanoprobe solution, corresponding to the presence of the antibodies. **c**, SDS-PAGE profile of a nanoprobe solution following ten-fold concentration using a 10-KDa cut-off

centrifugal filter (Amicon Ultra-0.5 10 KDa, Millipore Sigma). The catalytically active nanoprobe solution shows a typical high molecular weight protein band corresponding to the monoclonal antibody used in the fabrication process. **d**, Fourier-transform infrared spectroscopy (FTIR) of PtNPs and anti-HBV nanoprobe. Characteristic absorption peaks at 1635.0 cm^{-1}, 1552.7 cm^{-1}, and 1404.6 cm^{-1} were differentially observed in the nanoprobe solution when compared to the PtNPs suspension alone, and correspond to vibrations attributed to Amide I and Amide II (C=O stretching, N-H bending, C-N stretching), typical for the presence of antibodies. **e-f**, Zeta potential and Transmission Electron Microscopy (TEM) of the PtNPs. Zeta potential was performed using a Malvern Zetasizer (Malvern Instruments, Malvern, UK). Transmission electron microscope images were obtained using a JOEL 2100 TEM microscope at an acceleration voltage of 300 kV. PtNPs were spherical in shape with diameters of 3.78 ±1.125 nm with (scale bar = 10 nm). **g**, Field emission scanning electron microscopy (FE-SEM) images were acquired with the Zeiss instrument (resolution 1 nm, applied voltage 10-180 kV) on freshly prepared samples on a metallic sample holder. The size of the nanoprobe combined was about 23 nm. **h-i**, To test the abilities of the PtNPs and the fabricated nanoprobes in decomposing hydrogen peroxide, we performed H_2O_2-decomposition tests using an assay based on the optical absorption of hydrogen peroxide at λ= 240 nm[1] (h), and a highly sensitive colorimetric based assay (λmax = 570 nm) using horseradish peroxidase (HRP)-mediated reduction of H_2O_2 (Abcam, Cambridge, MA, US) (i). One microliter of a citrate-caped platinum nanoparticles suspension, containing *ca.* 1.3 x 10^{13} nanoparticles, showed a significant decrease in the absorption of a 5% H_2O_2 solution (1.63 M) over the course of a 10 min. kinetic assay (h). A similar decrease in absorption was observed for the enzymatic disproportionation of H_2O_2 by a native catalase from *Aspergillus niger* (Sigma-Aldrich) (h, small chart). Additionally, a ten-fold concentrated nanoprobe solution showed an H_2O_2-decomposition activity (average = 18.1%) comparable to the activity of the PtNPs stock solution (average = 20.8%) after 10 min. reaction with 0.1 mM H_2O_2, as measured by reduction in HRP-mediated conversion of the OxiRed probe (absorbance at 570 nm) when compared to the negative control (i). A positive control containing *A. niger* native catalase showed an average 50.9% reduction in the OxiRed probe color conversion during the same reaction time.

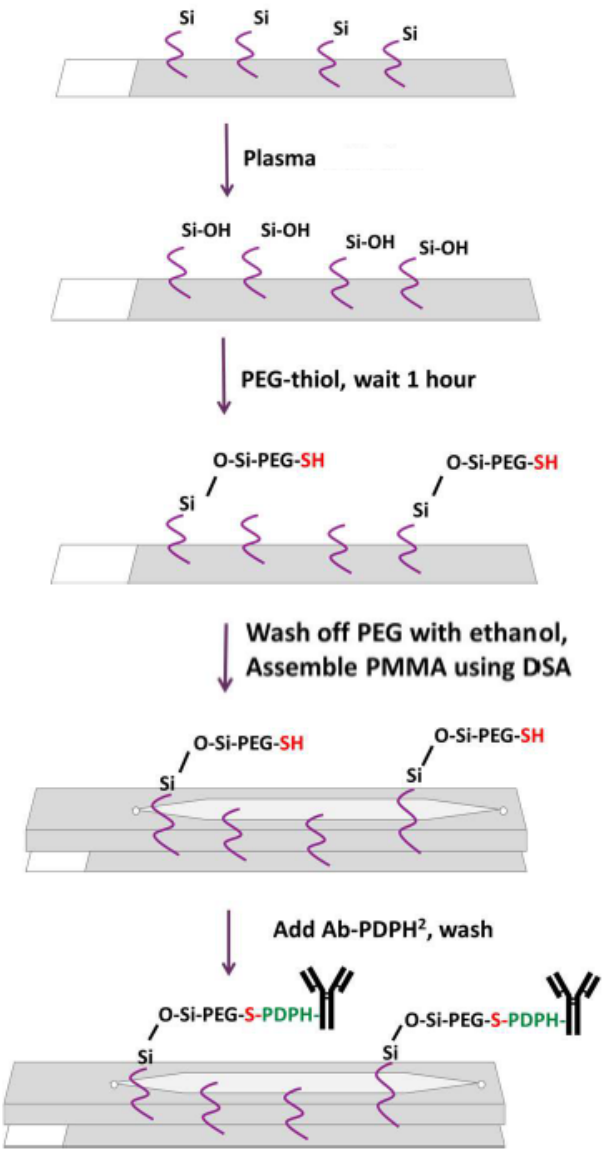

Figure S3. Schematic of microchip surface functionalization. PDPH = heterobifunctional crosslinking reagent 3-[2-Pyridyldithio]propionyl hydrazide. PMMA = 3.175 mm thick Poly(methyl methacrylate) sheet (8560K239, McMaster-Carr); DSA = double-sided adhesive (DSA) sheet (76 µm, 8213, 3M / or 125 µm, 8215, 3M). PEG-thiol = silane-PEG-thiol (20 mg/mL; Nanocs, cat. no. PG2-SLTH-5k).

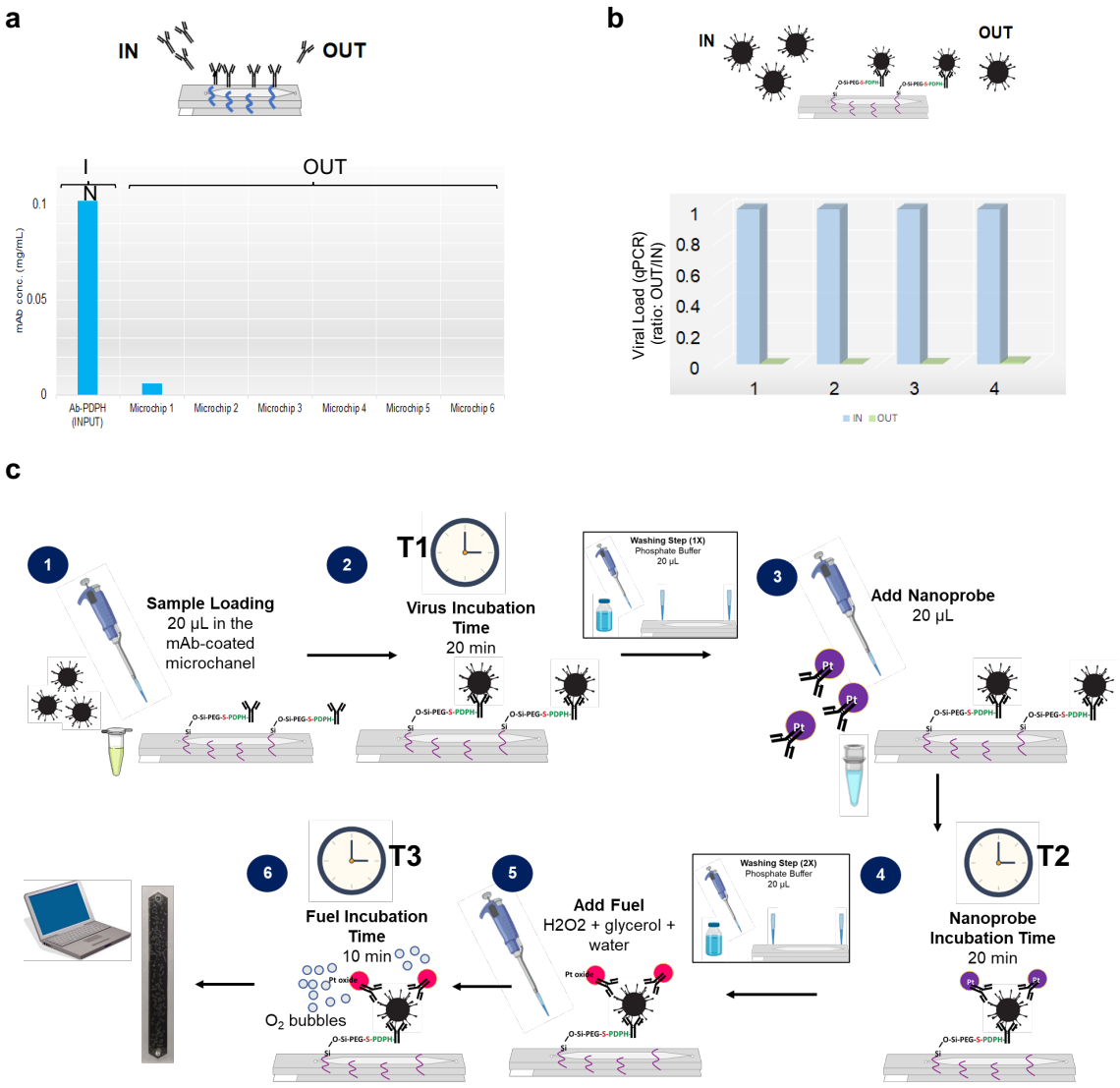

Figure S4. Efficiencies of antibody immobilization and virus capture in the surface of functionalized microchips, and detailed protocol for virus capture. a, Antibody concentrations before and after adding to the surface functionalized microchip were measured spectrophotometrically in different microchips (n = 6). **b**, HBV microchips were tested with viral concentrations between 10^3 and 10^6 IU/mL. Viral loads were quantitated by real-time quantitative PCR before and after loading the samples in the microchips. Results shown are the ratio OUT / IN of quantitated viral loads (n = 4 samples). **c**, The overall protocol used for detection of HBV, HIV, HCV, and SARS-CoV-2. The schematic shown is exactly the one used for HBV and HCV. For HIV and SARS-CoV-2, the virus incubation time (T1, step 2) was 45 min.

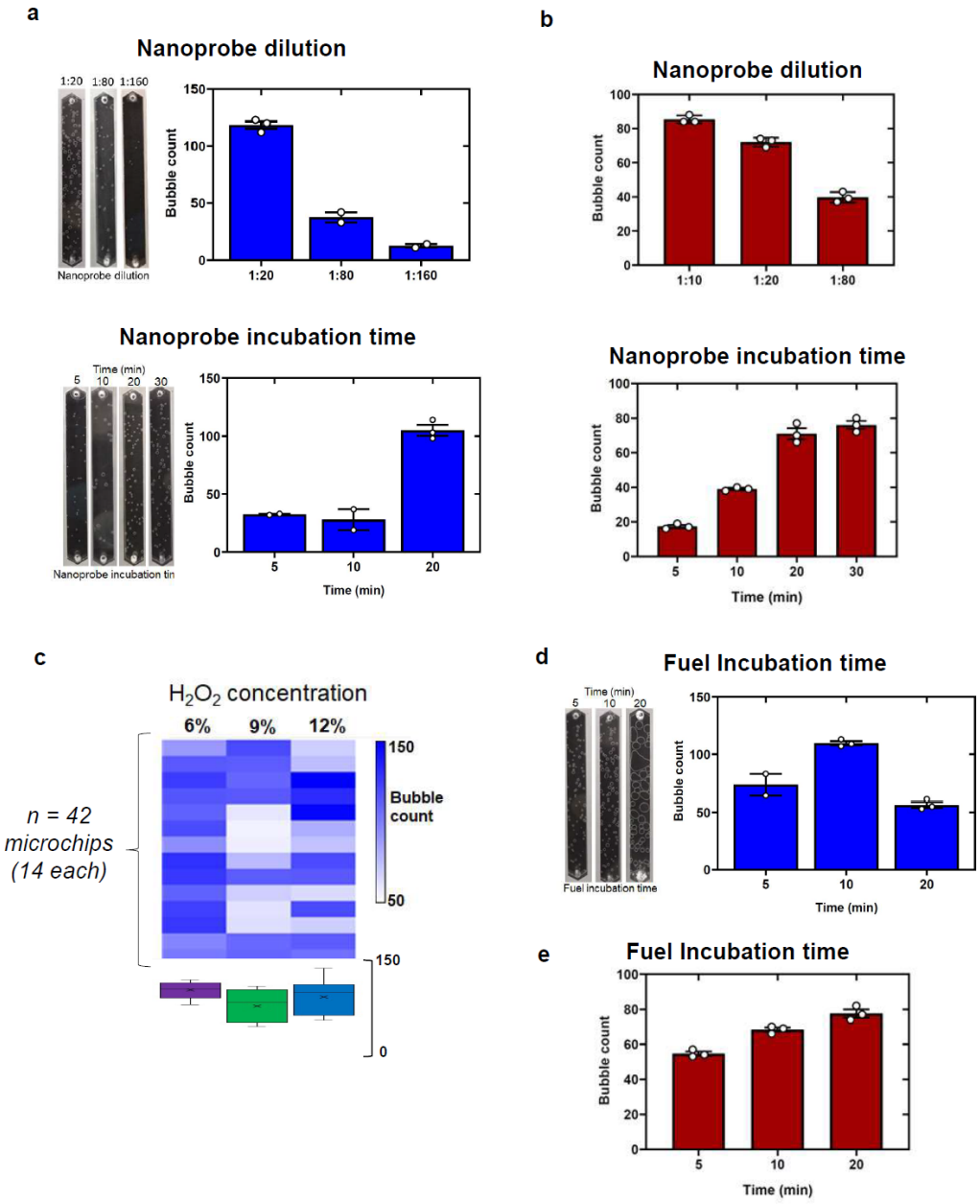

Figure S5. Standardization steps involved in the virus capture assay development. a, Nanoprobe dilution and incubation time used for the HBV detection assay, tested with HBV-spiked serum samples. **b**, Nanoprobe dilution and incubation time used for the HIV detection assay, tested with HIV-spiked serum samples. **c**, Stability of the bubbles detected in the microfluidic channels after 10 min incubation of the anti-HBV nanoprobe with a H_2O_2 fuel solution at different concentrations. Most stable bubbles are counted at 6% H_2O_2. d-e, Fuel incubation times in the HBV (d) and HIV (e) assays. The final incubation times of nanoprobes and fuel were 20 min and 10 min, respectively, for all viruses (HBV, HCV, HIV, SARS-CoV-2).

a

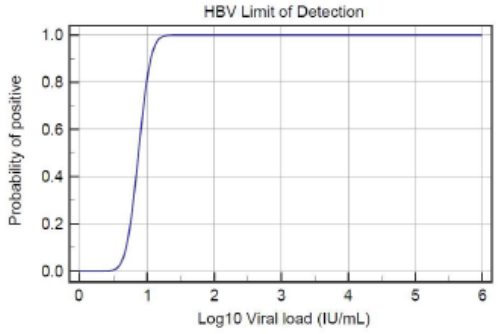

Method	Calculated limit of detection
Probit regression	99% probability of positives above 16 IU/mL
LLOD*	6 IU/ mL

b

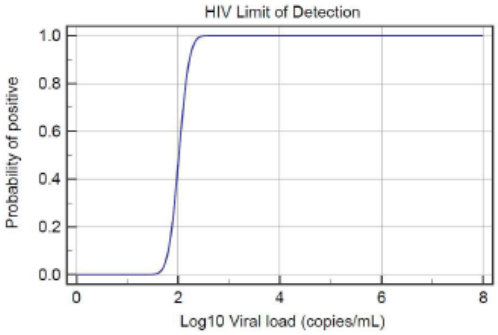

Method	Calculated limit of detection
Probit regression	99% probability of positives above 250 cps/mL
LLOD*	25 cps/mL

c

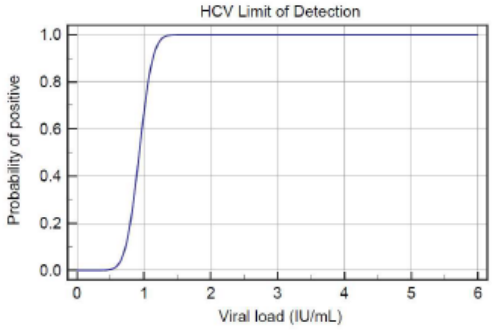

Method	Calculated limit of detection
Probit regression	99% probability of positives above 20 IU/mL
LLOD*	11 IU/mL

Figure S6. Probit regression analysis for definition of the assay's limits of detection. a-c, Calculations of limits of detections for the three different intact virus detection assays (HBV, HIV, HCV). The probabilities of positive for given samples at each point of the sigmoid curves are shown. The number of virus-spiked samples used for these calculations were: HBV (n = 87); HIV (n = 83); HCV (n = 25). Lowest limit of detection (LLOD) were considered as the lowest values that could differentiate positive samples from the negative controls, considering the Limit of Blank (LOB), calculated according to (Robb et al., 2019)[2].

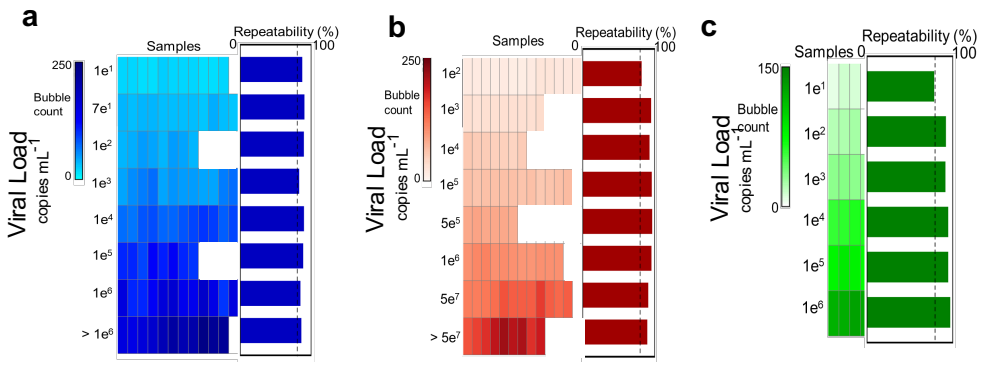

Figure S7. Repeatability of the antigen detection assays for HBV, HIV, and HCV, at various viral concentrations. Assay formats using microchips functionalized for capturing HBV (a), HIV (b), and HCV (c). Heatmaps show bubble counts obtained for individual samples, at various viral loads. Percentage coefficients of repeatability for each dilution are shown as bars. Vertical dashed lines mark 80.0%.

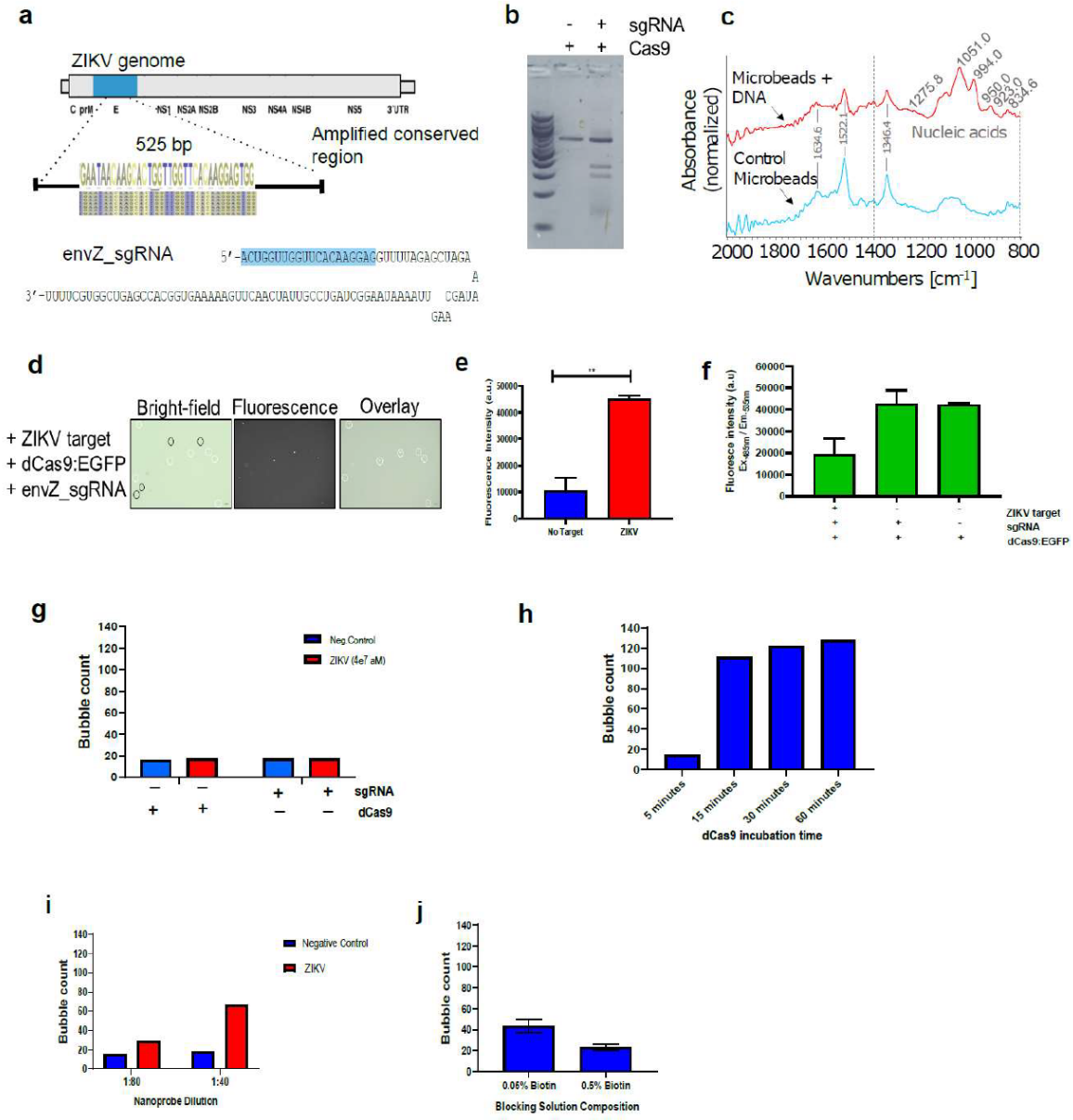

Figure S8. Standardization of the CRISPR/dCas9-based nucleic acid detection assay. a, We firstly designed a single guide RNA (envZ_sgRNA) targeting a highly conserved region of the envelope protein-encoding sequence in the Zika virus (ZIKV) genome. We also designed biotinylated oligonucleotide primers aimed at generating biotin-modified amplified products after reverse-transcription PCR from the specific ZIKV genomic region. **b**, To confirm the specific recognition of the ZIKV env target region by Cas9 using the designed sgRNA (envZ_sgRNA), a Cas9 nuclease assay using an enzymatically active form of the enzyme was performed using a

1:10:10 molar ratio of a target synthetic ZIKV DNA:sgRNA:Cas9. Only incubation with Cas9 in the presence of the designed envZ_sgRNA can induce a specific cut of the target ZIKV synthetic sequence (672 bp), generating bands at 289 bp and 383 bp, then confirming the ability of the ribonucleoprotein complex to recognize the nucleic acid of interest. **c**, To confirm that the amplified biotin-modified synthetic fragment of ZIKV was efficiently immobilized in the microbeads, we performed FT-IR analysis of the microbeads after binding of the env_Z biotinylated fragment, in comparison to control streptavidin-coated microbeads. There was a clear change in the FT-IR spectrum in the specific region where nucleic acid vibration groups are expected (mostly between 800cm-1 and 1400 cm-1). Major absorption peaks appeared at around 1275, 1051, 950-1009, 923, and 834 cm-1, which correlates well with most intense absorption peaks found in various previous studies, including vibrations corresponding to C-O deoxyribose stretching, C-C and C-O deoxyribose skeletal motions of DNA, deoxyribose-phosphate, and markers of B-form DNA[3,4]. Particularly, the most intense peak at 1051.0 has been previously shown as a marker of DNA dehydration, what corroborates our finding as the DNA-coated microbeads where resuspended in ethanol and left to dry on the surface of the crystal. **d-f**, We evaluated the ability of dCas9 to specifically detect the amplified target of interest when immobilized in the streptavidin-microbeads. For this, we used an EGFP-coupled chimeric dCas9 enzyme and detected the green fluorescence in the DNA-coated beads by fluorescence microscopy (d) and fluorimetry (e-r). Incubation in the presence of the specific sgRNA generated microbeads with detectable fluorescence only when the target sequence was immobilized (d-e), and the fluorescence was excluded from the solution when a magnetic rack was used to precipitate the microbeads (f). **g-j**, To standardize the bubble signal generation and detection in the microfluidic channel, we tested different times of incubation with the complex dCas9:sgRNA, different compositions of blocking solutions and washing steps, different dilutions of the specific anti-Cas9 nanoprobe, and different concentrations of hydrogen peroxide in the fuel solution.

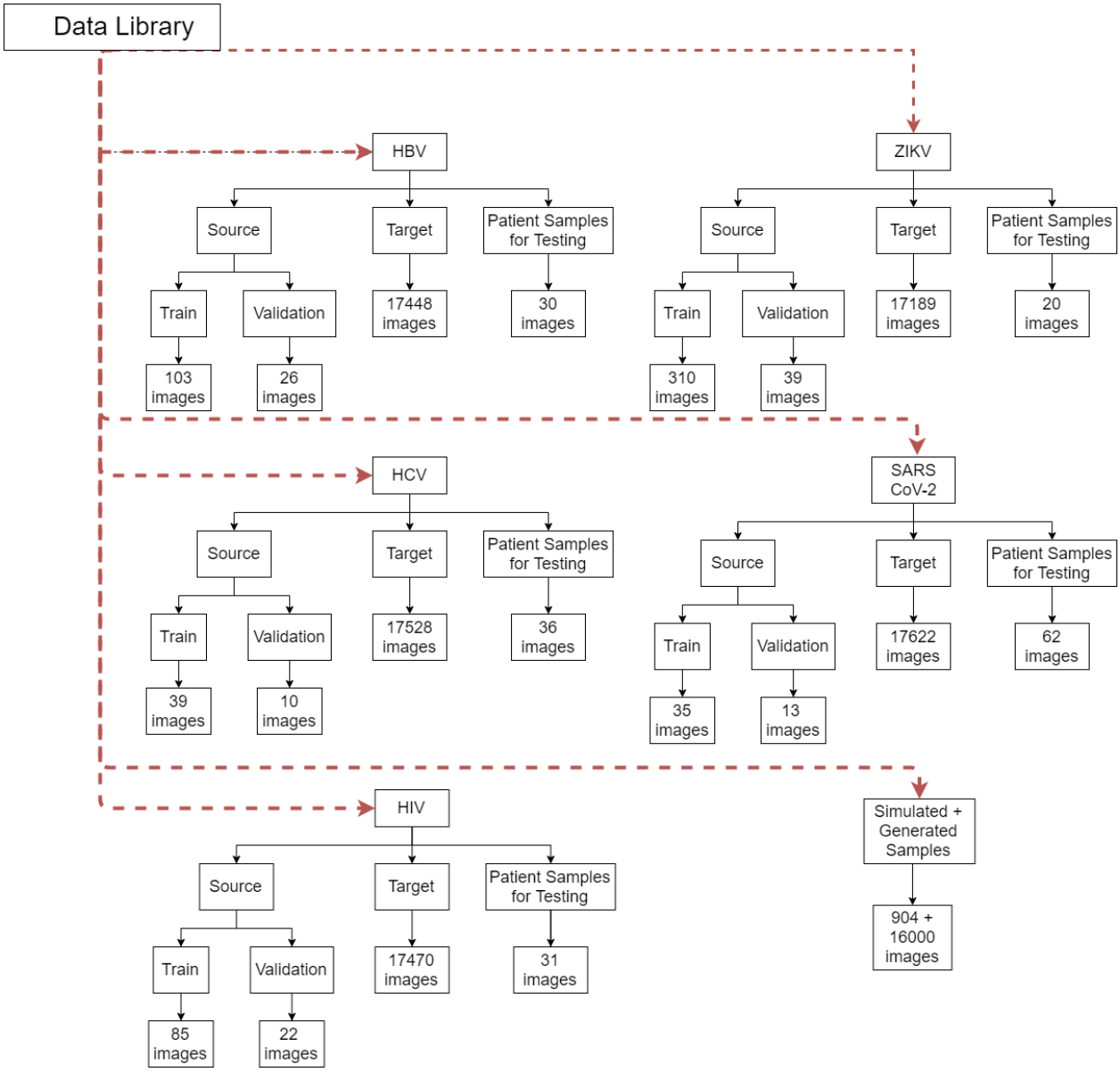

Figure S9. Organization of the smartphone-taken microchip image dataset. All specialist-annotated microchip images generated in the intact virus and nucleic acid detection assays were organized in five different domains – HBV (B), HIV (I), HCV (C), SARS-CoV-2 (C19), and ZIKV (Z) – alongside with a sixth domain containing unlabeled simulated samples (S). Flowchart showing the domain adaptation tasks. The five domains were sub-divided in *Source (SD)* domains (containing annotated image data for *Train* and *Validation* sets), and *Target (TD)* domains, containing unlabeled data with large feature distributions, encompassing bubbles of various shapes, sizes, concentrations and positions along the microfluidic channel. We followed standard protocols for domain adaptation in that we used all labeled source examples and all unlabeled target examples and performed five transfer learning tasks.

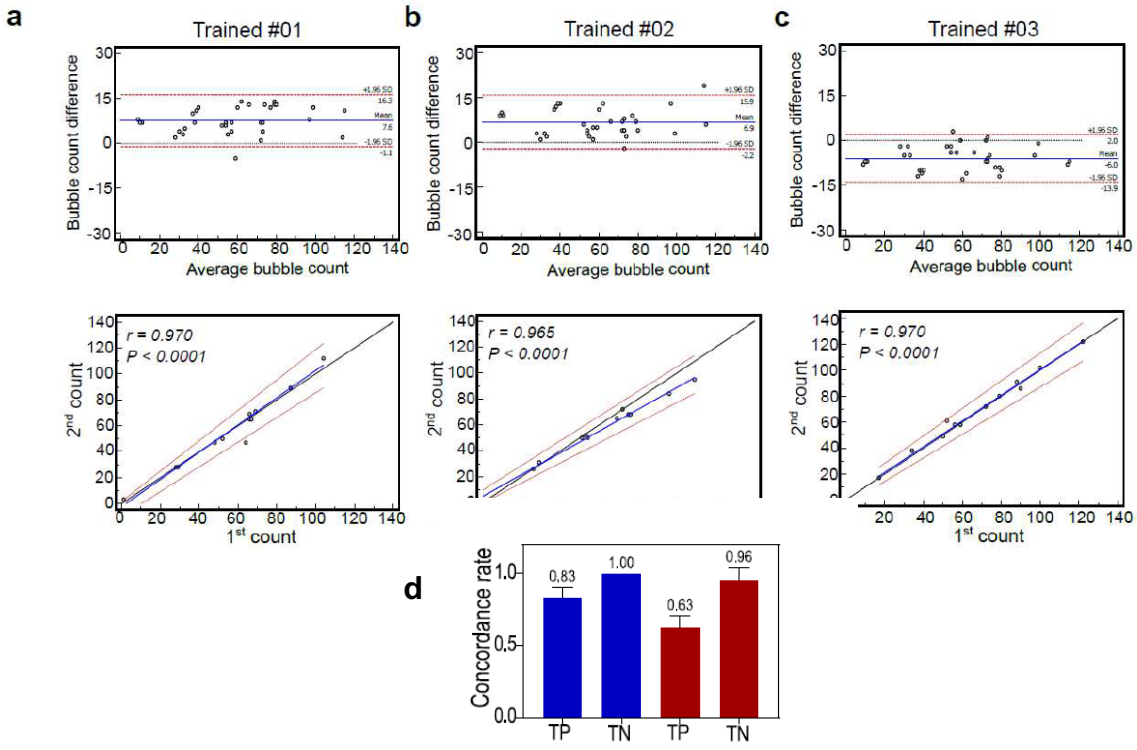

Figure S10. Consistency of image classification by trained specialists and untrained individuals, using bubble counts. a-c (upper panels), Bland-Altman plots comparing bubble counts obtained by each trained specialist (n = 3), with a reference count obtained using ImageJ (n=48). **a-c (lower panels)**, Intra-rater consistency was blindly tested with repeat microchip images presented to the specialists during the test and then counts in the first and second measurements were compared by Passing-Bablok regression analysis. **d**, Untrained individuals (n = 4) blindly rated microchip images as negative or positive (n = 36). Blue and red represent microchips from different viruses (HBV or HIV). TP = true positives; TN = true negatives.

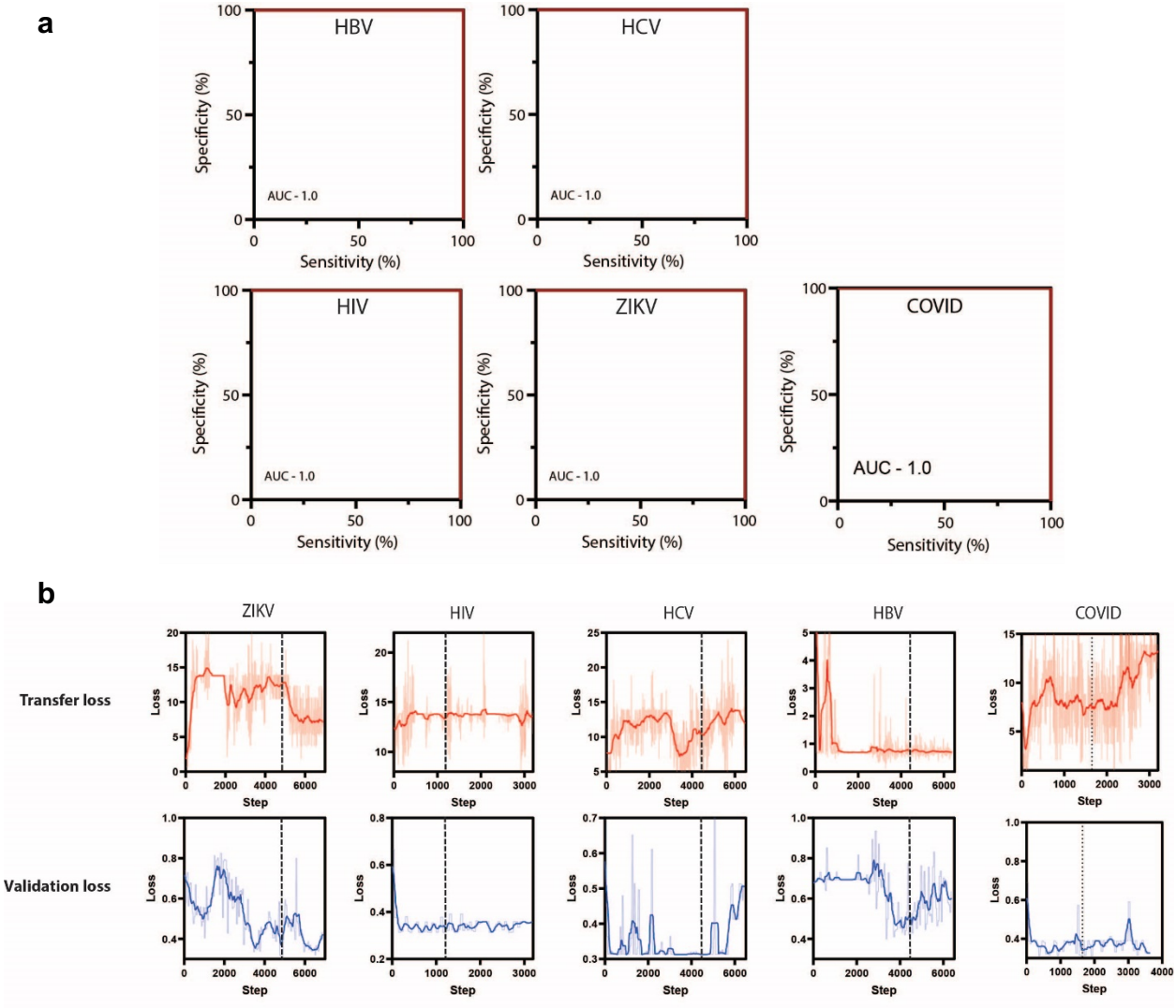

Figure S11. Overall performance of the adversarial neural networks with conditioning-based image classifiers. Receiver Operating Characteristic [5] curve analysis illustrating the separation capability of the adversarial network models based on the status of viral infection, using microchip-assay outcome images of patient samples. **b**, The transfer and validation loss curves of each adversarial model during the training cycle. Networks were saved at the lowest validation loss. The dotted lines indicate the saved model weights for each target.

a

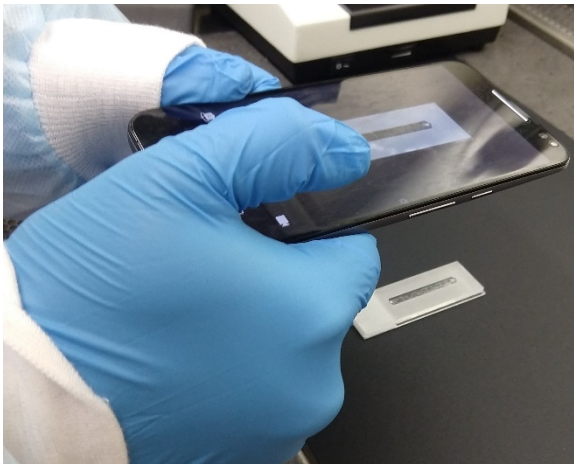

b

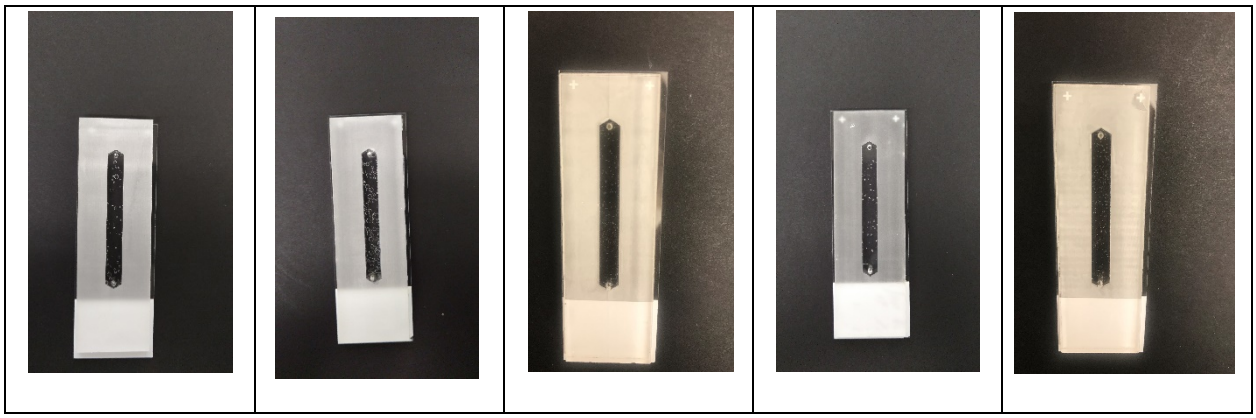

c

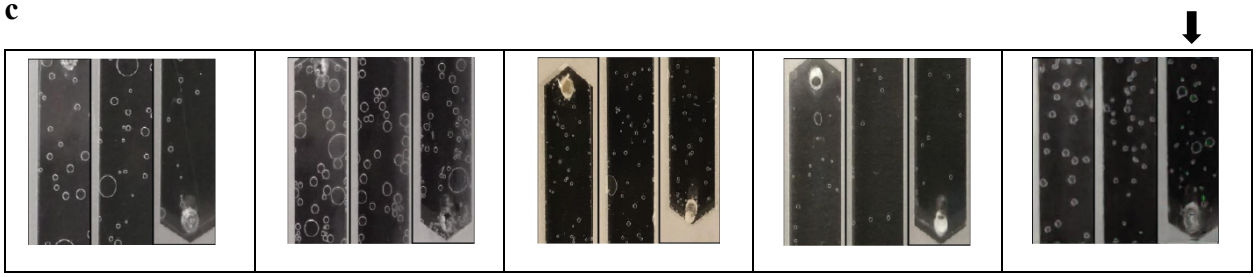

Figure S12. The microchip imaging procedure and examples of the image library. (a) Microchip imaging was done using the smartphone's rear camera, under normal ambient lighting conditions. The cellphone was positioned at a distance so as to permit imaging of the entire microchannel, with sufficient visibility of the bubbles. No other particular condition was required. (b) Examples of the microchip image library, showing variable numbers and shapes of bubbles, ambient illumination conditions and image sizes. (c) Isolated microchip channels showing bubbles of different shapes and sizes. The arrow indicates an image synthetically generated using StyleGANs.

Table S1. Overview of the performance of the adversarial neural networks with conditioning-based image classifiers.

	HBV	HIV	HCV	SARS-CoV-2	ZIKV
Source images	n= 129	n= 107	n= 49	n= 48	n= 349
Target images	n= 17,448	n= 17,470	n= 17,528	n= 17,622	n= 17,189
Patient samples[a]	n= 30	n= 31	n= 36	n= 62	n= 20
Sensitivity (%)	100% (CI: 78.20% to 100.00%)	100.00% (CI: 80.49% to 100.00%)	100.00% (CI: 83.89% to 100.00%)	100.00% (CI: 87.66% to 100.00%)	83.33% (CI: 51.59% to 97.91%)
Specificity (%)	100% (CI: 78.20% to 100.00%)	100.00% (CI: 76.84% to 100.00%)	100.00% (CI: 78.20% to 100.00%)	100.00% (CI: 89.72% to 100.00%)	100.00% (CI: 63.06% to 100.00%)
Accuracy	100.00% (CI: 88.43% to 100.00%)	100.00% (CI: 88.78% to 100.00%)	100.00% (CI: 90.26% to 100.00%)	100.00% (CI: 94.22% to 100.00%)	90% (CI: 68.30% to 98.77%)
PPV	100%	100.00%	100.00%	100.00%	100.00%
NPV	100%	100.00%	100.00%	100.00%	80% (CI: 53.02% to 93.41%)

[a] These numbers refer to the total numbers of patient samples tested in each assay format (including positive and negative samples). For the exact numbers of patient samples that are specifically positive of each virus, please see Table S3.

Table S2. Comparison of SPyDERMAN with CDC qRT-PCR assay for the detection of SARS-CoV-2.

	SPyDERMAN	**CDC qRT-PCR**
Target	Intact virus – spike protein	N gene (N1, N2, and N3)
LoD	1000 copies/ml	1000 copies/ml
Assay sample-to-result time	75 minutes	4 h including RNA extraction
Assay results	Qualitative	Quantitative
Assay components	On-chip virus capture (45 min at room temperature), Labeling captured viruses using PtNPs (20 min at room temperature), Bubble formation (10 min at room temperature), and optical signal read out and analysis using a cellphone camera.	UDG digestion (25 °C, 2 min), reverse transcription (50 °C, 15 min), denature (95 °C, 2 min) amplification, (95 °C, 3 s; 55 °C 30 s; 45 cycles)
Bulky instrumentation required	No	Yes

Table S3. Detailed information about the patient samples used in this study.

HBV patient samples					
Sample #	**Donor code**	**Gender**	**Origin**	**Additional characteristics**	**Viral Load (IU/mL) (qPCR)**
1	KH19-086977	N/A	USA		4,383,293
2	DLS17-038198	N/A	France	HBV: Genotype C	1,069,373
3	DLS17-038199	N/A	France	HBV: Genotype C	8,407,621
4	DLS17-038201	N/A	France	HBV: Genotype D	88,167,700
5	DLS13-01425	N/A	Vietnam	HBV: Genotype B	441,000
6	DLS14-06861	N/A	Vietnam	HBV: Genotype B | C	1,280,000
7	DLS14-06862	N/A	Vietnam		176,599
8	KH18-55281	N/A	USA		23
9	KH19-078194	N/A	USA		143
10	DLS17-038205	N/A	France	HBV: Genotype C	>110,000,000
11	DLS17-038211	N/A	France	HBV: Genotype F	192

12	DLS17-038212	N/A	France	HBV: Genotype E	7,199,505
13	DLS17-038209	N/A	France	HBV: Genotype D	13,961,137
14	DLS14-07957	N/A	Vietnam	HBV: Genotype B	2,960,000
15	DLS14-07958	N/A	Vietnam	HBV: Genotype B	3,490,000
16	DLS14-07959	N/A	Vietnam		341,051
17	DLS14-07961	N/A	Vietnam	HBV: Genotype B	27,200
18	DLS14-07963	N/A	Vietnam	HBV: Genotype B	10,200,000

HCV patient samples

Sample #	Donor code	Gender	Origen	Additional characteristics	Viral Load (IU/mL) (qPCR)
1	LDR0113	M	N/A	N/A	3,280
2	LDR0072	M	N/A	N/A	5,420
3	LDR0077	F	N/A	N/A	15,000
4	LDR0137	M	N/A	N/A	113,000
5	LDR0021	F	N/A	N/A	164,000
6	LDR0027	F	N/A	N/A	193,000
7	LDR0050	F	N/A	N/A	202,000
8	LDR0087	F	N/A	N/A	230,000
9	LDR010	M	N/A	N/A	248,000
10	LDR0074	F	N/A	N/A	491,000
11	LDR0101	M	N/A	N/A	506,000
12	LDR0013	F	N/A	N/A	868,000
13	LDR0122	F	N/A	N/A	1,020,000
14	LDR0120	M	N/A	N/A	1,040,000
15	LDR0140	F	N/A	N/A	4,470,000
16	LDR0100	M	N/A	N/A	4,610,000
17	LDR0104	M	N/A	N/A	5,880,000
18	LDR0039	F	N/A	N/A	6,020,000
19	LDR0026	F	N/A	N/A	26,700
20	LDR0180	M	N/A	N/A	875,000
21	LDR0090	M	N/A	N/A	670,000

HIV patient samples

Sample #	Donor code	Gender	Origen	Additional characteristics	Viral Load (cps/mL) (qPCR)
1	DLS0054630	N/A	USA	N/A	18,060
2	DLS0054640	N/A	USA	N/A	700
3	DLS0054641	N/A	USA	N/A	4,377
4	DLS0056261-S	N/A	USA	N/A	1,420
5	DLS0056264-S	N/A	USA	N/A	2,950
6	DLS0056266-S	N/A	USA	N/A	21,660
7	DLS0056272-S	N/A	USA	N/A	75,900
8	DLS0116319	N/A	USA	N/A	535,000
9	DLS0116321	N/A	USA	N/A	2,590,000
10	DLS13-11694	N/A	France	N/A	759
11	DLS0056269-S	N/A	France	N/A	32,070
12	DLS13-11720	N/A	France	N/A	8,245
13	DLS13-11721	N/A	France	N/A	16,112
14	DLS13-11728	N/A	France	N/A	6,565
15	DLS13-11729	N/A	France	N/A	10,657
16	DLS13-11731	N/A	France	N/A	27,326
17	DLS16-34350	N/A	USA	N/A	11,010
18	DLS16-34353	N/A	USA	N/A	5,520
19	DLS16-34363	N/A	USA	N/A	18,610

SARS-CoV-2 patient samples

Sample #	Donor code	Gender	Origen	Additional characteristics	Viral Load (cps/mL) (qPCR)
1	S00552266	N/A	N/A	N/A	187
2	S00552268	N/A	N/A	N/A	546,000,000
3	S00552269	N/A	N/A	N/A	490,000,000
4	S00552270	N/A	N/A	N/A	655
5	S00552271	N/A	N/A	N/A	9,110,000
6	S00552273	N/A	N/A	N/A	14,968,839
7	S00552274	N/A	N/A	N/A	1192
8	S00552275	N/A	N/A	N/A	28,554
9	S00552275	N/A	N/A	N/A	47,489,198

10	S00552276	N/A	N/A	N/A	12,085
11	S00552277	N/A	N/A	N/A	1,485
12	S00552278	N/A	N/A	N/A	1,072,463
13	S00552279	N/A	N/A	N/A	229,851,399
14	S00552280	N/A	N/A	N/A	427,999
15	S00552281	N/A	N/A	N/A	52
16	S00552282	N/A	N/A	N/A	87,700,000
17	S00552283	N/A	N/A	N/A	142,000,000
18	S00552284	N/A	N/A	N/A	17,200,000
19	S00552285	N/A	N/A	N/A	332,000,000
20	S00552286	N/A	N/A	N/A	46,300,000
21	S00552287	N/A	N/A	N/A	282,000,000
22	S00552288	N/A	N/A	N/A	26,800,000
23	S00552289	N/A	N/A	N/A	161,000,000
24	S00552291	N/A	N/A	N/A	436,000,000
25	S00552292	N/A	N/A	N/A	348
26	S00552293	N/A	N/A	N/A	750,000,000
27	S00552294	N/A	N/A	N/A	90,400,000
28	S00552295	N/A	N/A	N/A	274,000
29	S000552276-1	N/A	N/A	Diluted sample of S00552276 – used for assay standardization	3,000
30	S000552276-2	N/A	N/A	Diluted sample of S00552276 - used for assay standardization	3,000
31	S000552276-3	N/A	N/A	Diluted sample of S00552276 - used for assay standardization	3,000
32	S000552276-4	N/A	N/A	Diluted sample of S00552276 - used for assay standardization	3,000
33	S000552276-5	N/A	N/A	Diluted sample of S00552276 - used for assay standardization	5,000

34	S000552274-1	N/A	N/A	Diluted sample of S00552274 - used for assay standardization	5,000
35	S000551975	N/A	N/A	N/A	Negative
36	S000551976	N/A	N/A	N/A	Negative
37	S000551977	N/A	N/A	N/A	Negative
38	S000551978	N/A	N/A	N/A	Negative
39	S000551979	N/A	N/A	N/A	Negative
40	S000551980	N/A	N/A	N/A	Negative
41	S000551981	N/A	N/A	N/A	Negative
42	S000551982	N/A	N/A	N/A	Negative
43	S000551983	N/A	N/A	N/A	Negative
44	S000551984	N/A	N/A	N/A	Negative
45	S000551985	N/A	N/A	N/A	Negative
46	S000551986	N/A	N/A	N/A	Negative
47	S000551987	N/A	N/A	N/A	Negative
48	S000551988	N/A	N/A	N/A	Negative
49	S000551989	N/A	N/A	N/A	Negative
50	S000551990	N/A	N/A	N/A	Negative
51	S000551991	N/A	N/A	N/A	Negative
52	S000551992	N/A	N/A	N/A	Negative
53	S000551993	N/A	N/A	N/A	Negative
54	S000551994	N/A	N/A	N/A	Negative
55	S000551995	N/A	N/A	N/A	Negative
56	S000551996	N/A	N/A	N/A	Negative
57	S000551997	N/A	N/A	N/A	Negative
58	S000551998	N/A	N/A	N/A	Negative
59	S000551999	N/A	N/A	N/A	Negative
60	S000552000	N/A	N/A	N/A	Negative
61	S000552001	N/A	N/A	N/A	Negative
62	S000552002	N/A	N/A	N/A	Negative
63	S000552003	N/A	N/A	N/A	Negative
64	S000552004	N/A	N/A	N/A	Negative
65	AI900387949032220DD	N/A	N/A	N/A	Influenza B swab
66	AI900384151031120DD	N/A	N/A	N/A	Influenza B swab
67	AI900387954032020DD	N/A	N/A	N/A	Influenza A swab
68	AI900387955031920DD	N/A	N/A	N/A	Influenza A swab

ZIKV patient samples					
Sample #	**Donor code**	**Gender**	**Origen**	**Additional characteristics**	**Viral Load (Ct) (qPCR)**
1	D000011743	F	Dominican Republic	Aptima Zika Virus Assay (0)	Not detected
2	D000011752	F	Dominican Republic	Aptima Zika Virus Assay (0)	Not detected
3	D000013839	F	Dominican Republic	Aptima Zika Virus Assay (33.74)	Medium VL
4	D000010409	M	Dominican Republic	Aptima Zika Virus Assay (0)	Medium VL
5	D000012068	F	Dominican Republic	Aptima Zika Virus Assay (33.2)	Medium VL
6	D000011942	M	Dominican Republic	Aptima Zika Virus Assay (31.93)	High VL

Table S4. List of antibodies, oligonucleotides, and synthetic nucleic acids used in this study

1. Antibodies				
Name	**Target**	**Characteristics**	**Used in:**	**Provider**
anti-HBV	HBV surface antigen (HBsAg)	B521M monoclonal antibody (mAb)	HBV intact virus detection assay	Genetex, cat. no. GTX41736
Anti-HCV	HCV core antigen (HCV cAg)	6A1 mAb	HCV intact virus detection assay	Abcam, cat. no. ab2582
Anti-HIV1 (1)	HIV envelope glycoprotein (gp120)	2557 mAb	HIV intact virus detection assay	NIH AIDS Reagent Program, cat. no. 13429
Anti-HIV1 (2)	HIV envelope glycoprotein (gp120)	goat anti-HIV1 gp120 pAb	HIV intact virus detection assay	Abcam, cat. no. ab21179
Anti-SARS-CoV-2	SARS-CoV-2 (2019-nCoV) Spike S1 Antibody	Rabbit MAb	SARS-COV-2 intact virus detection assay	Sino Biological, cat. no. 40150-R007
anti-Cas9 mAb	CRISPR associated protein 9 from *S. pyogenes*	Cas9 mAb	CRISPR/dCas9 detection assay	Applied Biological Materials, abm, cat. no. Y300079
2. Oligonucleotides				
Name	**Sequence (5' – 3')**	**Characteristics**	**Used in:**	**Provider**

ZK_F	TGCTGTCAGTTCATGGCTCC	20-mer; 5' – Biotin	Amplification of conserved ZIKV *env* region	IDT Technologies
ZK_R	TGAATGTGAACGCTGCGGTA	20-mer; 5' – Biotin	Amplification of conserved ZIKV *env* region	IDT Technologies
DEN_F	GTGACATTTAAAACAGCTCATGC	23-mer; 5' – Biotin	Amplification of conserved DENV *env* region	IDT Technologies
DEN_R	CTTTCACCAAAAGGCGGTTC	20-mer; 5' – Biotin	Amplification of conserved DENV *env* region	IDT Technologies
3. Synthetic DNA fragments				
Name	**Sequence (5' – 3')**	**Characteristics**	**Used in:**	**Provider**
env_Z	GTGACATGCGCTAAGTTTGCATGCTCCAAGAAAATGACCGGGAAGAGCATCCAGCCAGAGAATCTGGAGTACCGGATAATGCTGTCAGTTCATGGCTCCCAGCACAGTGGGATGATCGTTAATGACACAGGACATGAAACTGATGAGAATAGAGCGAAGGTTGAGA TAACGCCCAATTCACCAAGAGCCGAAGCCACCCTGGGGGGTTTTGGAAGCCTAGGACTTGATTGTGAACCGAGGACAGGCCTTGACTTTTCAGATTTGTATTACTTGACTATGAATAACAAGCACTGGTTGGTTCACAAGGAGTGGTTCCACGACATTCCATTACCTTGGCACGCTGGGGCAGACACCGGAACTCCACACTGGAACAACAAAGAAGCACTGGTAGAGTTCAAGGACGCACATGCCAAAAGGCAAACTGTCGTGGTTCTAGGGAGTCAAGAAGGAGCAGTTCACACGGCCCTTGCTGGAGCTCTGGAGGCTGAGATGGATGGTGCAAAGGGAAGGCTGTCCTCTGGCCACTTGAAATGTCGCCTGAAAATGGATAAACTTAGATTGAAGGGCGTGTCATACTCCTTGTGTACCGCAGCGTTCACATTCACCAAG	Conserved portion of the ZIKV Env-encoding region	Standardization of CRISPR/dCas9 based assay	IDT Technologies

	ATCCCGGCTGAAACACTGCAC GGGACAGTCACAGTGGAGGTA CAGTACGCAGGGACAGATGGA			
DEN1	AGACAAGATTTGCTGGTGACA TTTAAAACAGCTCATGCAAAG AAGCAAGAAGTAGTCGTACTA GGATCACAAGAAGGAGCAAT GCACACTGCGCTGACCGGAGC GACGGAAATCCAAACGTCTGG AACGACAACAATTTTTGCAGG ACACTTGAAATGTAGACTAAA GATGGACAAACTGACTCTAAA AGGGATGTCATATGTGATGTG CACAGGCTCATTCAAGCTAGA GAAAGAAGTGGCTGAGACCCA GCATGGAACCGTTCTAGTGCA GATCAAATACGAAGGAACAG ATGCACCATGCAAGATTCCTT TTTCGACCCAAGATGAAAAAG GAGTAACCCAGAATGGGAGAT TGATAACAGCCAACCCCATAG TCACTGATAAAGAAAAACCAG TCAACATTGAGGCAGAACCGC CTTTTGGTGAAAGTTACATCGT GATAG	Conserved portion of the DENV Env-encoding region	Standardization of CRISPR/dCas9 based assay	IDT Technologies
DEN2	AGAAAGAAATGCTAGTAACAT TCAAAAACCCCCATGCGAAAA GACAAGACGTTGTCGTCTTGG GATCGCAAGAGGGCGCCATGC ACACAGCACTCACAGGCCGGC AACAGAAATTCAGATGTCATC GGGAAATATACTATTTATGGG GCATTTGAAGTGTAGACTGAG GATGGACAAGCTGCAACTCAA AGGGATGTCGTACTCCATGTG CACAGGAAAGTTCAAAGTTGT CAAAGAAATAGCAGAAACAC AACATGGAACGATAGTCATCA GAGTGCAGTATGAAGGAGAA GACTCACCGTGCAAGATCCCT TTTGAGATCATGGACTTGGAA AAGAAACATGTCTTAGGGCGA CTGATTACGGTCAACCCAATA GTGATAGGGAAAGACAGCCCA ATCAACATAGAAGCAGAACCT	Conserved portion of the DENV Env-encoding region	Standardization of CRISPR/dCas9 based assay	IDT Technologies

	CCTTTTGGTGACAGCTATATTG TCATA			
DEN3	AGGAAGGAGCTTCTTGTGACA TTCAAAAACGCACATGCGAAA AAACAAGAAGTAGTTGTCCTT GGATCGCAAGAGGGAGCAAT GCATACAGCACTGACAGGAGC CACAGAAATCCAAAACTCAGG AGGCACAAGCATTTTTGCGGG GCACTTAAAATGTAGACTTAA GATGGACAAATTGGAACTCAA GGGGATGAGCTATGCAATGTG CACGAATACCTTTGTGTTGAA GAAAGAAGTCTCAGAAACGCA GCATGGGACAATACTCGTTAA AGTCGAGTACAAAGGGGAAG ATGCACCTTGCAAGATTCCTTT CTCCACAGAGGATGGACAAGG GAAAGCTCACAATGGCAGACT GATCACAGCCAACCCAGTGGT GACTAAGAAGGAGGAGCCTGT CAATATTGAGGCTGAACCTCC TTTTGGGGAAAGTAATATAGT AATTG	Conserved portion of the DENV Env-encoding region	Standardization of CRISPR/dCas9 based assay	IDT Technologies
DEN4	ATAAAGAGAGAATGGTGACAT TCAAGGTTCCTCATGCCCAAG AGACAGGATGTGACAGTGCTA GGATCTCAGGAGGGAGCTATG CATTCTGCCCTCGCCGGAGCC ACAGAAGTAGATTCTGGTGAT GGAAATCACATGTTTGCAGGA CATCTCAAGTGCAAAGTCCGC ATGGAGAAATTGAGAATTAAA GGAATGTCATACACGATGTGT TCAGGAAAGTTCTCAATTGAC AAAGAGATGGCAGAAACACA G CATGGAACTACAGTGGTGAAA GTCAAGTATGAAGGCGCTGGA GCTCCGTGTAAAGTCCCCATA GAGATAAGAGATGTGAACAA GGAAAAAGTGGTCGGACGTAT CATCTCATCTACCCCTTTTGCT GAGAATACCAACAGCGTAACC AACATAGAATTAGAACCCCCT	Conserved portion of the DENV Env-encoding region	Standardization of CRISPR/dCas9 based assay	IDT Technologies

	TTTGGGGACAGCTACATAGTG ATAG			
4. sgRNA				
Name	**crRNA sequence, without PAM (5' – 3')**	**Characteristics**	**Used in:**	**Provider**
Env_sgR NA	ACTGGTTGGTTCACAAGGAG	Single molecule sgRNA.	CRISPR/Cas9 mediated detection of amplified ZIKV genomic region	IDT Technologies

References used in the supplementary information:

1 Li, Y.; Schellhorn, H. E. Rapid Kinetic Microassay for Catalase Activity. *J. Biomol. Tech.* **2007**, *18*, 185-187.

2 Robb, N. C.; Taylor, J. M.; Kent, A.; Pambos, O. J.; Gilboa, B.; Evangelidou, M.; Mentis, A.F.; Kapanidis, A.N. Rapid Functionalisation and Detection of Viruses *vi*a a Novel Ca(2+)-Mediated Virus-DNA Interaction. *Sci. Rep.* **2019**, *9*, 16219, DOI:10.1038/s41598-019-52759-5.

3 Mello, M. L.; Vidal, B. C. Changes in the Infrared Microspectroscopic Characteristics of DNA Caused by Cationic Elements, Different Base Richness and Single-Stranded Form. *PLoS One* **2012**, *7*, e43169, DOI:10.1371/journal.pone.0043169.

4 Al-Jorani, K.; Ruther, A.; Martin, M.; Haputhanthri, R.; Deacon, G.B.; Li, H.L.; Wood, B. The Application of ATR-FTIR Spectroscopy and the Reversible DNA Conformation as a Sensor to Test the Effectiveness of Platinum(II) Anticancer Drugs. *Sensors* **2018**, *18*, DOI:10.3390/s18124297 (2018).

5 Ganin, U. E.; Ajakan, H.; Germain, P., Larochelle, H.; Laviolette, F.; Marchand, M.; Lempitsky, V. Domain-Adversarial Training of Neural Networks. *J. Mach. Learn. Res.* **2016**, *17*, 35.

6 CDC. Real-Time RT–PCR Panel for Detection 2019-nCoV (US Centers for Disease Control and Prevention, 2020); Available at: https://www.cdc.gov/coronavirus/2019-ncov/lab/ RT-PCR-detection-instructions.html. (2020).